

Delayed X- and Gamma-Ray Line Emission from Solar Flare Radioactivity

V. Tatischeff

CSNSM, IN2P3-CNRS and Université Paris-Sud, F-91405 Orsay Cedex, France

tatische@csnsm.in2p3.fr

B. Kozlovsky

School of Physics and Astronomy, Tel Aviv University, Ramat Aviv, Tel Aviv 69978, Israel

J. Kiener

CSNSM, IN2P3-CNRS and Université Paris-Sud, F-91405 Orsay Cedex, France

and

R. J. Murphy

*E. O. Hulburt Center for Space Research, Code 7650, Naval Research Laboratory, Washington,
DC 20375*

ABSTRACT

We have studied the radioactive line emission expected from solar active regions after large flares, following the production of long-lived radioisotopes by nuclear interactions of flare-accelerated ions. This delayed X- and gamma-ray line emission can provide unique information on the accelerated particle composition and energy spectrum, as well as on mixing processes in the solar atmosphere. Total cross sections for the formation of the main radioisotopes by proton, ^3He and α -particle reactions are evaluated from available data combined with nuclear reaction theory. Thick-target radioisotope yields are provided in tabular form, which can be used to predict fluxes of all of the major delayed lines at any time after a gamma-ray flare. The brightest delayed line for days after the flare is found to be the 511 keV positron-electron annihilation line resulting from the decay of several β^+ radioisotopes. After ~ 2 days however, the flux of the e^+e^- annihilation line can become lower than that of the 846.8 keV line from the decay of ^{56}Co into ^{56}Fe . Our study has revealed other delayed gamma-ray lines that appear to be promising for detection, e.g. at 1434 keV from the radioactivity of both the isomer $^{52}\text{Mn}^m$ ($T_{1/2}=21.1$ min) and the ground state $^{52}\text{Mn}^g$ ($T_{1/2}=5.59$ days), 1332 and 1792 keV from ^{60}Cu ($T_{1/2}=23.7$ min), and 931.1 keV from ^{55}Co ($T_{1/2}=17.5$ hours). The strongest delayed X-ray line is found to be the Co $K\alpha$ at 6.92 keV, which is produced from both the decay of the isomer $^{58}\text{Co}^m$ ($T_{1/2}=9.04$ hours) by the conversion of a

K-shell electron and the decay of ^{57}Ni ($T_{1/2}=35.6$ hours) by orbital electron capture. Prospects for observation of these lines with *RHESSI* or future space instruments are discussed.

Subject headings: nuclear reactions, nucleosynthesis, abundances – Sun: flares – Sun: X-rays, gamma rays

1. Introduction

Gamma-ray lines from solar flares were first observed in 1972 with the gamma-ray spectrometer (GRS) aboard the *OSO-7* satellite (Chupp et al. 1973). Since then, repeated observations with various space missions, including the *Solar Maximum Mission*/GRS (e.g. Share & Murphy 1995), all four *Compton Gamma Ray Observatory* instruments (e.g. Share, Murphy, & Ryan 1997) and the *Reuven Ramaty High Energy Solar Spectroscopic Imager* (*RHESSI*; e.g. Lin et al. 2003), have firmly established gamma-ray astronomy as an important tool for studying the active sun. Prompt gamma-ray lines are produced from deexcitation of nuclei excited by nuclear interactions of flare-accelerated particles with the solar atmosphere. Detailed spectroscopic analyses of this emission have furnished valuable information on the composition of the ambient flare plasma, as well as on the composition, energy spectrum and angular distribution of the accelerated ions (e.g. Ramaty & Mandzhavidze 2000; Share & Murphy 2001; Lin et al. 2003; Kiener et al. 2006). Additional information about the density and temperature of the ambient plasma is obtained from the positron-electron annihilation line at 0.511 MeV (Murphy et al. 2005) and the neutron capture line at 2.223 MeV (Hua et al. 2002 and references therein).

The bombardment of the solar atmosphere by flare-accelerated ions can also synthesize radioactive nuclei, whose decay can produce observable, delayed gamma-ray lines in the aftermath of large flares. One of the most promising of such lines is at 846.8 keV resulting from the decay of ^{56}Co (half-life $T_{1/2}=77.2$ days) into the first excited state of ^{56}Fe (Ramaty & Mandzhavidze 2000; Kozlovsky, Murphy, & Ramaty 2002). Ramaty & Mandzhavidze (2000) calculated the time dependence of the 846.8 keV line emission that would have been expected after the 6 X-class flares of June 1991. Smith et al. are now searching for this delayed line emission with the *RHESSI* spectrometer after the very intense series of flares that occurred between 2003 October 28 and November 4 (the analysis is in progress, D. Smith 2006, private communication).

The observation of solar radioactivity can be important for at least two reasons. First, the radioisotopes can serve as tracers to study mixing processes in the solar atmosphere (Ramaty & Mandzhavidze 2000). Additionally, their detection should provide a new insight into the spectrum and fluence of flare-accelerated ions. In particular, since the accelerated heavy nuclei are believed to be significantly enhanced as compared to the ambient medium composition (e.g. Murphy et al. 1991), the radioisotopes are expected to be predominantly produced by interactions of fast heavy ions with ambient hydrogen and helium. Thus, the delayed line emission can provide a valuable

measurement of the accelerated metal enrichment.

We performed a systematic study of the radioactive line emission expected after large solar flares. In addition to gamma-ray lines emitted from deexcitation of daughter nuclei, we considered radioactivity X-ray lines that can be produced from the decay of proton-rich isotopes by orbital electron capture or the decay of isomeric nuclear levels by emission of a conversion electron. We also treated the positron-electron annihilation line resulting from the decay of long-lived β^+ -emitters. The radioisotopes which we studied are listed in Table 1, together with their main decay lines. We selected radioactive X- and gamma-ray line emitters that can be significantly produced in solar flares (see § 2) and with half-lives between ~ 10 min, which is the typical duration of large gamma-ray flares (Vestrand et al. 1999), and 77.2 days (^{56}Co half-life). We neglected radioisotopes with mean lifetime τ_r greater than that of ^{56}Co , because (1) their activity ($\dot{N}_r = N_r/\tau_r$) is lower and (2) their chance of surviving at the solar surface is also lower.

In § 2, we present the total cross sections for the production of the most important radioactive nuclei. In § 3, we describe our thick-target yield calculations of the radioisotope synthesis. The results for the delayed line emission are presented in § 4. Prospects for observations are discussed in § 5.

2. Radioisotope production cross sections

All of the radioactive nuclei shown in Table 1 can be significantly produced in solar flares by H and He interactions with elements among the most abundant of the solar atmosphere and accelerated particles: He, C, N, O, Ne, Mg, Al, Si, S, Ar, Ca, Cr, Mn, Fe and Ni¹. We did not consider the production of radioisotopes with atomic number $Z > 30$. We also neglected a number of very neutron-rich nuclei (e.g. ^{28}Mg , ^{38}S ...), whose production in solar flares should be very low.

Most of the radioisotopes listed in Table 1 are proton-rich, positron emitters. Their production by proton and α -particle reactions with the abundant constituents of cosmic matter was treated in detail by Kozlovsky, Lingenfelter, & Ramaty (1987). The work of these authors was extended by Kozlovsky, Murphy, & Share (2004) to include β^+ -emitter production from the most important reactions induced by accelerated ^3He . However, new laboratory measurements have allowed us to significantly improve the evaluation of a number of cross sections for the production of important positron emitters. In the following, we present updated cross sections for the formation of $^{34}\text{Cl}^m$, $^{52}\text{Mn}^g$, $^{52}\text{Mn}^m$, ^{55}Co , ^{56}Co , ^{57}Ni , $^{58}\text{Co}^g$, ^{60}Cu , and ^{61}Cu , by proton, ^3He and α reactions in the

¹Kuzhevskij, Gan, & Miroshnichenko (2005) recently claimed that nuclear interactions between fast and ambient heavy nuclei can be important for the formation of rare isotopes in solar flares. We evaluated the significance of these reactions by using the universal parameterization of total reaction cross sections given by Tripathi, Cucinotta, & Wilson (1996). Assuming a thick target interaction model, a power-law source spectrum for the fast ions and standard compositions for the ambient and accelerated nuclei (see § 3), we found that the heavy ion collisions should contribute less than a few percent of the total radioisotope production and can therefore be safely neglected.

energy range 1–10³ MeV nucleon⁻¹. In addition, we evaluate cross sections for the production of the 4 radioactive nuclei of Table 1 which are not positron emitters: ⁷Be, ²⁴Na, ⁵⁶Mn and ⁵⁸Co^m.

The reactions which we studied are listed in Table 2. We considered proton, ³He and α -particle interactions with elements of atomic numbers close to that of the radioisotope of interest and that are among the most abundant of the solar atmosphere. Spallation reactions with more than 4 outgoing particles were generally not selected, because their cross sections are usually too low and their threshold energies too high to be important for solar flares. We generally considered reactions with elements of natural isotopic compositions, because, except for H and the noble gases, the terrestrial isotopic compositions are representative of the solar isotopic abundances (Lodders 2003). Furthermore, most of the laboratory measurements we used were performed with natural targets.

Most of the cross section data were extracted from the EXFOR database for experimental reaction data². When laboratory measurements were not available or did not cover the full energy range, we used 3 different nuclear reaction codes to obtain theoretical estimates. Below a few hundred MeV (total kinetic energy of the fast particles), we performed calculations with both EMPIRE-II (version 2.19; Herman et al. 2004) and TALYS (version 0.64; Koning, Hilaire, & Duijvestijn 2005). These computer programs account for major nuclear reaction models for direct, compound, pre-equilibrium and fission reactions. They include comprehensive libraries of nuclear structure parameters, such as masses, discrete level properties, resonances and gamma-ray parameters. The TALYS and EMPIRE-II calculations were systematically compared with available data and the agreement was generally found to be better than a factor of 2. We obtained, however, more accurate predictions for isomeric cross sections with TALYS than with EMPIRE-II.

Above the energy range covered by TALYS and EMPIRE-II, we used the "Silberberg & Tsao code" (Silberberg, Tsao, & Barghouty 1998 and references therein) when experimental cross section data for proton-nucleus spallation reactions were lacking. This code is based on the semiempirical formulation originally developed by Silberberg & Tsao (1973) for estimates of cross sections needed in cosmic-ray physics. It has been updated several times as new cross sections measurements have become available (Silberberg et al. 1998). For spallation reactions induced by α -particles above ~ 100 MeV nucleon⁻¹, we used the approximation (Silberberg & Tsao 1973)

$$\sigma_{\alpha}(E) = X\sigma_p(4E) , \tag{1}$$

where E is the projectile kinetic energy per nucleon, σ_{α} and σ_p are the cross sections for the α -particle- and proton-induced reactions leading to the same product, and

$$X = \begin{cases} 1.6 & \text{for } \Delta A \lesssim 3 \\ 2 & \text{for } \Delta A > 3 , \end{cases} \tag{2}$$

where ΔA is the difference between target and product masses.

²See <http://www.nndc.bnl.gov/exfor/>.

2.1. ${}^7\text{Be}$ Production

The relevant cross sections for ${}^7\text{Be}$ production are shown in Figure 1. The cross section for the reaction ${}^4\text{He}(\alpha, n){}^7\text{Be}$ (dashed curve labeled “ ${}^4\text{He}$ ” in Fig. 1) is from the measurements of King et al. (1977) from 9.85 to 11.85 MeV nucleon $^{-1}$ and Mercer et al. (2001 and references therein) above ~ 15.4 MeV nucleon $^{-1}$. The cross sections for the proton reactions with ${}^{12}\text{C}$, ${}^{14}\text{N}$ and ${}^{16}\text{O}$ (solid curves in Fig. 1) are from the extensive measurements of Michel et al. (1997 and references therein). The cross sections for the α -particle reactions with ${}^{12}\text{C}$, ${}^{14}\text{N}$ and ${}^{16}\text{O}$ (dashed curves labeled “ ${}^{12}\text{C}$ ”, “ ${}^{14}\text{N}$ ” and “ ${}^{16}\text{O}$ ” in Fig. 1) are from the measurements of Lange et al. (1995) below 42 MeV nucleon $^{-1}$ and from TALYS calculations at 50 and 62.5 MeV nucleon $^{-1}$. At higher energies, we used the data compilation of Read & Viola (1984) and assumed the ${}^7\text{Be}$ production cross sections to be half of the isobaric cross sections for producing the mass $A=7$ fragment from spallation of the same target isotope. The cross section for the reaction ${}^{12}\text{C}({}^3\text{He}, x){}^7\text{Be}$ (dotted curve in Fig. 1) is from Ditrói et al. (1994) below 9.1 MeV nucleon $^{-1}$ and from TALYS calculations from 10 to 83.3 MeV nucleon $^{-1}$. At higher energies, we extrapolated the cross section assuming the same energy dependence as the one for the ${}^{12}\text{C}(\alpha, x){}^7\text{Be}$ reaction. We neglected the production of ${}^7\text{Be}$ from ${}^3\text{He}$ reactions with ${}^{14}\text{N}$ and ${}^{16}\text{O}$.

2.2. ${}^{24}\text{Na}$ Production

The relevant cross sections for ${}^{24}\text{Na}$ production are shown in Figure 2. The cross section for the reaction ${}^{25}\text{Mg}(p, 2p){}^{24}\text{Na}$ is from Meadows & Holt (1951) below 105 MeV, Reeder (1969) in the energy range 105–300 MeV and above 400 MeV, and Korteling & Caretto (1970) at 300 and 400 MeV. The cross section for the reaction ${}^{26}\text{Mg}(p, 2pn){}^{24}\text{Na}$ is also from Meadows & Holt (1951) and Korteling & Caretto (1970) below 400 MeV. Its extrapolation at higher energies was estimated from calculations with the Silberberg & Tsao code. The cross sections for the proton reactions with ${}^{27}\text{Al}$ and ${}^{nat}\text{Si}$ are from the measurements of Michel et al. (1997). The cross section for the reaction ${}^{nat}\text{Mg}(\alpha, x){}^{24}\text{Na}$ is from the data of Lange et al. (1995) below 42 MeV nucleon $^{-1}$ and from TALYS calculations at 50 and 62.5 MeV nucleon $^{-1}$. Above 100 MeV nucleon $^{-1}$, the $\alpha+{}^{nat}\text{Mg}$ cross section was estimated from equations (1) and (2), and the $p+{}^{25}\text{Mg}$ and $p+{}^{26}\text{Mg}$ cross sections discussed above. The cross sections for the reactions ${}^{22}\text{Ne}(\alpha, pn){}^{24}\text{Na}$ and ${}^{22}\text{Ne}({}^3\text{He}, p){}^{24}\text{Na}$ are not available in the literature and were estimated from calculations with the TALYS and EMPIRE-II codes, respectively.

2.3. ${}^{34}\text{Cl}^m$ Production

Shown in Figure 3 are cross sections for production of the first excited (isomeric) state of ${}^{34}\text{Cl}$ (${}^{34}\text{Cl}^m$, $T_{1/2} = 32$ min) at an excitation energy of 146.4 keV. The cross section data for these reactions are scarce. The cross section for the reaction ${}^{32}\text{S}({}^3\text{He}, p){}^{34}\text{Cl}^m$ was measured by Lee &

Markowitz (1974) from 1.4 to ~ 7.3 MeV nucleon⁻¹. Its rapid fall at higher energies was estimated from TALYS calculations. The cross section of the reaction $^{34}\text{S}(p,n)^{34}\text{Cl}^m$ was measured by Hintz & Ramsey (1952) from threshold to ~ 90 MeV. However, as the decay scheme of ^{34}Cl was not well known in 1952, it is not clear which fraction of the isomeric state was populated in this experiment. We thus did not use these data, but have estimated the cross section from TALYS calculations. We also used theoretical evaluations from the TALYS and the Silberberg & Tsao codes for the reactions $^{32}\text{S}(\alpha,pn)^{34}\text{Cl}^m$ and $^{sol}\text{Ar}(p,x)^{34}\text{Cl}^m$. In this latter reaction, the notation ^{sol}Ar means Ar of solar isotopic composition³ and the cross section was obtained by weighting the cross sections for proton reactions with ^{36}Ar , ^{38}Ar and ^{40}Ar by the relative abundances of these three isotopes in the solar system.

2.4. $^{52}\text{Mn}^{g,m}$ Production

The production of the ground state of ^{52}Mn ($^{52}\text{Mn}^g$, $T_{1/2} = 5.59$ days) and of the isomeric level at 377.7 keV ($^{52}\text{Mn}^m$, $T_{1/2} = 21.1$ min) are both important for the delayed line emission of solar flares. The relevant cross sections are shown in Figure 4. The data for the production of the isomeric pair $^{52}\text{Mn}^g$ and $^{52}\text{Mn}^m$ in $p+^{nat}\text{Cr}$ collisions are from Wing & Huizenga (1962) from 5.8 MeV to 10.5 MeV; West, Lanier, & Mustafa (1987) from 6.3 to ~ 26.9 MeV; Klein, Roesch, & Qaim (2000) from ~ 17.4 to ~ 38.1 MeV; and Reuland & Caretto (1969) at 400 MeV. It is noteworthy that TALYS simulations for these reactions were found to be in very good agreement with the data, which demonstrates the ability of this code to predict accurate isomeric state populations. The cross section for the reaction $^{nat}\text{Fe}(p,x)^{52}\text{Mn}^g$ is from Michel et al. (1997). We estimated the cross section for the production of the isomer $^{52}\text{Mn}^m$ in $p+^{nat}\text{Fe}$ collisions by multiplying the cross section for the ground state production by the isomeric cross section ratio σ_m/σ_g calculated with the TALYS code. The cross sections for the production of $^{52}\text{Mn}^g$ and $^{52}\text{Mn}^m$ from $\alpha+^{nat}\text{Fe}$ interactions are also from TALYS calculations below 62.5 MeV nucleon⁻¹. They were extrapolated at higher energies using equations (1) and (2), and the $p+^{nat}\text{Fe}$ cross sections discussed above. Also shown in Figure 4 is the cross section for the reaction $^{nat}\text{Cr}(^3\text{He},x)^{52}\text{Mn}^m$, which is based on the data of Fessler, Alfassi, & Qaim (1994) below ~ 11.7 MeV nucleon⁻¹ and TALYS calculations at higher energies.

2.5. ^{56}Mn Production

The relevant cross sections for ^{56}Mn production are shown in Figure 5. The laboratory measurements for the production of this radioisotope are few. We used the experimental works of the following authors: Watanabe, Nakahara, & Murakami (1979) for the reaction $^{55}\text{Mn}(^3\text{He},2p)^{56}\text{Mn}$ from

³The solar isotopic composition of Ar and the other noble gases are very different from their terrestrial isotopic compositions (see Lodders 2003 and references therein).

~ 3.8 to ~ 12.9 MeV nucleon $^{-1}$; Michel, Brinkmann, & Stück (1983a) for the reaction $^{55}\text{Mn}(\alpha, 2pn)^{56}\text{Mn}$ from 6.1 to ~ 42.8 MeV nucleon $^{-1}$; and Michel, Brinkmann, & Stück (1983b) for the reaction $^{nat}\text{Fe}(\alpha, x)^{56}\text{Mn}$ from ~ 13.8 to ~ 42.8 MeV nucleon $^{-1}$. The excitation functions for these 3 reactions were completed by theoretical estimates from TALYS. The cross section for the reaction $^{57}\text{Fe}(p, 2p)^{56}\text{Mn}$ is entirely based on nuclear model calculations, from EMPIRE-II below 100 MeV and the Silberberg & Tsao code at higher energies.

2.6. ^{55}Co , ^{56}Co and ^{57}Ni Production

The relevant cross sections for production of ^{55}Co , ^{56}Co and ^{57}Ni are shown in Figures 6, 7 and 8, respectively. The cross sections for the proton reactions with ^{nat}Fe and ^{nat}Ni are based on the data of Michel et al. (1997). For ^{56}Co production by $p+^{nat}\text{Fe}$ and $p+^{nat}\text{Ni}$ collisions, we also used the works of Takács, Vasváry, & Tárkányi (1994) and Tárkányi, Szelecsényi, & Kopecky (1991), respectively. The cross sections for the α -particle reactions with ^{nat}Fe are from Tárkányi et al. (2003b) below 10.75 MeV nucleon $^{-1}$, Michel et al. (1983b) in the energy range ~ 12.3 – 42.8 MeV nucleon $^{-1}$ and TALYS calculations at 50 and 62.5 MeV nucleon $^{-1}$. These cross sections were extrapolated at higher energies assuming that they have energy dependences similar to those of the $p+^{nat}\text{Fe}$ reactions (see eqs. [1] and [2]). The cross sections for the α -particle reactions with ^{nat}Ni are based on the data of Michel et al. (1983b). For the reaction $^{nat}\text{Ni}(\alpha, x)^{57}\text{Ni}$, we also used the measurements of Takács, Tárkányi, & Kovacs (1996) below ~ 6.1 MeV nucleon $^{-1}$. The procedure to estimate the $\alpha+^{nat}\text{Ni}$ cross sections above 50 MeV nucleon $^{-1}$ was identical to the one discussed above for the $\alpha+^{nat}\text{Fe}$ cross sections. The cross sections for the ^3He reactions with ^{nat}Fe are based on the data of Tárkányi, Ditrói, & Takács (2003a) from ~ 4.1 to ~ 8.5 MeV nucleon $^{-1}$, the data of Hazan & Blann (1965) from 1.9 to ~ 19.8 MeV nucleon $^{-1}$, and TALYS calculations. The measurements of Hazan & Blann (1965) were performed with targets enriched in ^{56}Fe . To estimate the cross section for $^3\text{He}+^{nat}\text{Fe}$ collisions from their data, we multiplied the measured cross section by 0.92, the relative abundance of ^{56}Fe in natural iron. We neglected the production of ^{55}Co and ^{56}Co by $^3\text{He}+^{nat}\text{Ni}$ interactions. For the reaction $^{nat}\text{Ni}(^3\text{He}, x)^{57}\text{Ni}$, we used the data of Takács et al. (1995) below ~ 11.7 MeV nucleon $^{-1}$ and EMPIRE-II calculations to 80 MeV nucleon $^{-1}$. At higher energies, the cross section was extrapolated assuming an energy dependence similar to the one of the $^{nat}\text{Ni}(\alpha, x)^{57}\text{Ni}$ cross section.

2.7. $^{58}\text{Co}^{g,m}$ Production

The relevant cross sections for the production of the isomeric pair $^{58}\text{Co}^{g,m}$ are shown in Figures 9a and b. The isomeric state of ^{58}Co ($^{58}\text{Co}^m$, $T_{1/2} = 9.04$ hours) is the first excited level at 24.9 keV. It decays to the ground state by the conversion of a K-shell electron, thus producing a Co $K\alpha$ line emission at 6.92 keV. The ground state $^{58}\text{Co}^g$ having a much longer lifetime, $T_{1/2} = 70.9$ days, we considered for its production the total cross section for the formation of the

isomeric pair, $\sigma_t = \sigma_m + \sigma_g$. Isomeric cross section ratios σ_m/σ_t were measured for various reaction channels by Sudár & Qaim (1996 and references therein). We used their data for the reaction $^{55}\text{Mn}(\alpha, n)^{58}\text{Co}^{g,m}$ below ~ 6.3 MeV nucleon $^{-1}$. At higher energies, we used the σ_m and σ_t measurements of Matsuo et al. (1965) and Rizvi et al. (1989), respectively. The total cross section for the reaction $^{nat}\text{Fe}(\alpha, x)^{58}\text{Co}$ is based on the data of Iwata (1962) from 4.4 to 9.65 MeV nucleon $^{-1}$ and Michel et al. (1983b) in the energy range ~ 6.5 –42.8 MeV nucleon $^{-1}$. In the absence of data for the isomer formation in $\alpha + ^{nat}\text{Fe}$ collisions, we estimated the cross section by multiplying the cross section for the total production of ^{58}Co by the isomeric ratio σ_m/σ_t calculated with the TALYS code. The total cross section for the reaction $^{nat}\text{Fe}(^3\text{He}, x)^{58}\text{Co}$ is from Hazan & Blann (1965) and Tárkányi, Ditrói, & Takács (2003a) below ~ 8.5 MeV nucleon $^{-1}$. At higher energies, it is based on TALYS calculations. The cross section for the isomeric state population in $^3\text{He} + ^{nat}\text{Fe}$ collisions is also from simulations with the TALYS code.

The cross sections for $^{58}\text{Co}^{g,m}$ production from proton, ^3He and α reactions with ^{nat}Ni are shown in Figure 9b. The total cross sections σ_t are based on the data of Michel et al. (1997), Takács et al. (1995) below ~ 11.7 MeV nucleon $^{-1}$, and Michel et al. (1983b) below ~ 42.7 MeV nucleon $^{-1}$, for the proton, ^3He and α reactions, respectively. To extrapolate the cross sections for the ^3He and α reactions, we used the TALYS code and the approximation described by equations (1) and (2). Data for the isomeric state population are lacking and we estimated the σ_m cross sections as above, i.e. from TALYS calculations of the isomeric ratios σ_m/σ_t .

2.8. ^{60}Cu and ^{61}Cu Production

The relevant cross sections for the production of ^{60}Cu and ^{61}Cu are shown in Figure 10. The cross sections for the production of ^{60}Cu are based on the data of Barrandon et al. (1975) below ~ 17 MeV, Muramatsu et al. (1978) below ~ 8.8 MeV nucleon $^{-1}$, and Takács et al. (1995) below ~ 11.7 MeV nucleon $^{-1}$, for the proton, α -particle and ^3He reactions with ^{nat}Ni , respectively. The cross section for the reaction $^{nat}\text{Ni}(^3\text{He}, x)^{61}\text{Cu}$ is also from Takács et al. (1995) below ~ 11.7 MeV nucleon $^{-1}$. The cross section for the reaction $^{nat}\text{Ni}(\alpha, x)^{61}\text{Cu}$ was constructed from the data of Takács et al. (1996) below ~ 6.1 MeV nucleon $^{-1}$, Muramatsu et al. (1978) from ~ 2.5 to ~ 9.2 MeV nucleon $^{-1}$, and Michel et al. (1983b) in the energy range ~ 4.2 –42.7 MeV nucleon $^{-1}$. All these cross sections were extrapolated to higher energies by the means of TALYS calculations.

3. Radioisotope production yields

We calculated the production of radioactive nuclei in solar flares assuming a thick target interaction model, in which accelerated particles with given energy spectra and composition produce nuclear reactions as they slow down in the solar atmosphere. Taking into account the nuclear destruction and catastrophic energy loss (e.g. interaction involving pion production) of the fast

particles in the interaction region, the production yield of a given radioisotope r can be written as (e.g. Parizot & Lehoucq 1999):

$$Q_r = \sum_{ij} n_j \int_0^\infty \frac{dE v_i(E) \sigma_{ij}^r(E)}{\dot{E}_i(E)} \int_E^\infty dE' N_i(E') \exp \left[- \int_E^{E'} \frac{dE''}{\dot{E}_i(E'') \tau_i^{ine}(E'')} \right], \quad (3)$$

where i and j range over the accelerated and ambient particle species that contribute to the synthesis of the radioisotope considered, n_j is the density of the ambient constituent j , v_i is the velocity of the fast ion i , σ_{ij}^r is the cross section for the nuclear reaction $j(i,x)r$, \dot{E}_i is the energy loss rate for the accelerated particles of type i in the ambient medium, N_i is the source energy spectrum for these particles, and τ_i^{ine} is the energy dependent average lifetime of the fast ions of type i before they suffer inelastic nuclear collisions in the interaction region. As H and He are by far the most abundant constituents of the solar atmosphere, we have

$$\tau_i^{ine} \cong \frac{1}{v_i (n_H \sigma_{iH}^{ine} + n_{He} \sigma_{iHe}^{ine})}, \quad (4)$$

where σ_{iH}^{ine} and σ_{iHe}^{ine} are the total inelastic cross sections for particle i in H and He, respectively. We used the cross sections given by Moskalenko et al. (2002) for the p -H and p -He total inelastic reactions and the universal parameterization of Tripathi et al. (1996,1999) for the other fast ions.

The energy loss rate was obtained from

$$\dot{E}_i = v_i \frac{Z_i^2(\text{eff})}{A_i} \left[n_H m_H \left(\frac{dE}{dx} \right)_{pH} + n_{He} m_{He} \left(\frac{dE}{dx} \right)_{pHe} \right], \quad (5)$$

where $(dE/dx)_{pH}$ and $(dE/dx)_{pHe}$ are the proton stopping powers (in units of MeV g⁻¹ cm²) in ambient H and He, respectively (Berger et al. 2005), m_H and m_{He} are the H- and He-atom masses, $Z_i(\text{eff}) = Z_i [1 - \exp(-137\beta_i/Z_i^{2/3})]$ is the equilibrium effective charge (Pierce & Blann 1968), $\beta_i = v_i/c$ is the particle velocity relative to that of light, and Z_i and A_i are the nuclear charge and mass for particle species i , respectively. Inserting equations (4) and (5) into equation (3), we see that under the assumption of thick target interactions, the yields do not depend on the ambient medium density, but only on the relative abundances n_j/n_H . We used for the ambient medium composition the same abundances as Kozlovsky et al. (2004, Table 2).

We took for the source energy spectrum of the fast ions an unbroken power law extending from the threshold energies of the various nuclear reactions up to $E_{max}=1$ GeV nucleon⁻¹:

$$N_i(E) = C_i E^{-s} H(E_{max} - E), \quad (6)$$

where the function $H(E)$ denotes the Heaviside step function and C_i is the abundance of the accelerated particles of type i . We assumed the following impulsive-flare composition for the accelerated ions: we used for the abundances of fast C and heavier elements relative to α -particles the average composition of solar energetic particles (SEP) measured in impulsive events from interplanetary space (Reames 1999, Table 9.1), but we took the accelerated α/p abundance ratio to be 0.5, which

is at the maximum of the range observed in impulsive SEP events. The choice of such a large α/p ratio is motivated by analyses of gamma-ray flares (Share & Murphy 1997; Manzhavidze, Ramaty, & Kozlovsky 1997, 1999), showing a relatively strong emission in the line complex at ~ 450 keV from α -particle interactions with ambient ^4He . The expected modifications of our results for higher proton abundances relative to α -particles and heavier ions are discussed in § 4. We performed calculations with an accelerated $^3\text{He}/\alpha$ abundance ratio of 0.5, which is typical of the accelerated ^3He enrichment found in impulsive SEP events (Reames, Meyer, & von Roseninge 1994; Reames 1999), as well as in gamma-ray flares (Share & Murphy 1998; Manzhavidze et al. 1999). The resulting accelerated-particle composition is similar to the one used by Kozlovsky et al. (2004), but slightly less enriched in heavy elements (e.g. Fe and Ni abundances are lower than those of these authors by 13% and 29%, respectively). The enhancement of the fast heavy elements is however still large relative to the ambient material composition. We have, for example, $C_{Fe}/C_p = 137n_{Fe}/n_H$.

Thick-target radioisotope yields are given in Table 3 for $s=3.5$, 2 and 5 (eq. [6]). The first value is close to the mean of spectral index distribution as measured from analyses of gamma-ray line ratios (Ramaty, Mandzhavidze, & Kozlovsky 1996), whereas the two other values are extreme cases to illustrate the dependence of the radioisotope production on the spectral hardness. The calculations were normalized to unit incident number of protons of energy greater than 5 MeV. For comparison, the last two lines of this table give thick-target yields for the production of the 4.44 and 6.13 MeV deexcitation lines from ambient ^{12}C and ^{16}O , respectively. These prompt narrow lines are produced in reactions of energetic protons and α -particles with ambient ^{12}C , ^{14}N , ^{16}O and ^{20}Ne (see Kozlovsky et al. 2002). We can see that, relative to these two gamma-ray lines, the production of most of the radioisotopes increases as the accelerated particle spectrum becomes harder (i.e. with decreasing s). This is because the radioactive nuclei are produced by spallation reactions at higher energies, on average, than the ^{12}C and ^{16}O line emission, which partly results from inelastic scattering reactions.

Because of the enhanced heavy accelerated particle composition, most of the yield is from interactions of heavy accelerated particles with ambient H and He. For example, the contribution of fast Fe and Ni collisions with ambient H and He accounts for more than 90% of the total ^{56}Co production, whatever the spectral index s .

Because we are interested in emission after the end of the gamma-ray flare, we show in the fifth column of Table 3 a factor f_d which should be multiplied with the given yields to take into account the decay of the radioactive nuclei occurring before the end of the flare. It was calculated from the simplifying assumption that the radioisotope production rate is constant with time during the flare for a time period Δt . We then have

$$f_d = \frac{\tau_r}{\Delta t} (1 - e^{-\Delta t/\tau_r}), \quad (7)$$

where τ_r is the mean lifetime of radioisotope r . In Table 3, f_d is given for $\Delta t=10$ min.

4. Delayed X- and gamma-ray line emission

Calculated fluxes of the most intense delayed lines are shown in Tables 4–6 for three different times after a large gamma-ray flare. The lines are given in decreasing order of their flux for $s=3.5$. The calculations were normalized to a total fluence of the summed 4.44 and 6.13 MeV prompt narrow lines $\mathcal{F}_{4.4+6.1}=300$ photons cm^{-2} , which is the approximate fluence observed in the 2003 October 28 flare with *INTEGRAL*/SPI (Kiener et al. 2006). The flux of a given delayed line l produced by the decay of a radioisotope r at time t after the end of the nucleosynthesis phase was obtained from

$$F_l(t) = \frac{\mathcal{F}_{4.4+6.1} Q_r f_d I_l^r}{Q_{4.4+6.1} \tau_r} e^{-t/\tau_r}, \quad (8)$$

where Q_r and $Q_{4.4+6.1}$ are the yields (Table 3) of the parent radioisotope and summed prompt ^{12}C and ^{16}O lines, respectively, and I_l^r is the line branching ratio (the percentages shown in Table 1). The factor f_d was calculated for a flare duration of 10 min (Table 3). The calculated fluxes do not take into account attenuation of the line photons in the solar atmosphere. Unless the flare is very close to the solar limb, the attenuation of the delayed gamma-ray lines should not be significant (see Hua, Ramaty, & Lingenfelter 1989) as long as the radioactive nuclei do not plunge deep in the solar convection zone. The delayed X-ray lines can be more significantly attenuated by photoelectric absorption (see below).

A full knowledge of the delayed 511 keV line flux would require a comprehensive calculation of the accelerated particle transport, solar atmospheric depth distribution of β^+ -emitter production and transport of the emitted positrons, because (1) the number of 2γ line photons produced per emitted positron (f_{511}) crucially depends on the density, temperature and ionization state of the solar annihilation environment (Murphy et al. 2005), (2) significant escape of positrons from the annihilation region can occur, and (3) the line can be attenuated by Compton scattering in the solar atmosphere. Here, we simply assumed $f_{511}=1$ (see Kozlovsky et al. 2004; Murphy et al. 2005) and neglected the line attenuation. We see in Tables 4 and 5 that the annihilation line is predicted to be the most intense delayed line for hours after the flare end. After ~ 2 days however, its flux can become lower than that of the 846.8 keV line from the decay of ^{56}Co into ^{56}Fe (see Table 6). We show in Figure 11 the time dependence of the 511 keV line flux, for $s=3.5$ and $\Delta t=10$ min, together with the contributions of the main radioactive positron emitters to the line production. We see that from ~ 1 to ~ 14 hours, ^{18}F is the main source of the positrons. Since this radioisotope can be mainly produced by the reaction $^{16}\text{O}(^3\text{He},p)^{18}\text{F}$, we suggest that a future detection of the decay curve of the solar 511 keV line could provide an independent measurement of the flare-accelerated ^3He abundance. Prompt line measurements have not yet furnished an unambiguous determination of the fast ^3He enrichment (Manzhavidze et al. 1997).

Among the 9 atomic lines listed in Table 1, the most promising appears to be the Co $K\alpha$ line at 6.92 keV (Tables 4–5). It is produced from both the decay of the isomer $^{58}\text{Co}^m$ by the conversion of a K-shell electron and the decay of ^{57}Ni by orbital electron capture. Additional important atomic lines are the Fe and Ni $K\alpha$ lines at 6.40 and 7.47 keV, respectively. The X-ray

line fluxes shown in Tables 4 and 5 should be taken as upper limits, however, because photoelectric absorption of the emitted X-rays was not taken into account, as it depends on the flare location and model of accelerated ion transport. Calculations in the framework of the solar magnetic loop model (Hua et al. 1989) showed that the interaction site of nuclear reactions is expected to be in the lower chromosphere, at solar depths corresponding to column densities of 10^{-3} to 10^{-1} g cm^{-2} . These results were reinforced by the gamma-ray spectroscopic analyses of Ramaty et al. (1995), who showed that the bulk of the nuclear reactions are produced in flare regions where the ambient composition is close to coronal, i.e. above the photosphere. For such column densities of material of coronal composition, we calculated from the photoelectric absorption cross sections of Balucinska-Church & McCammon (1992) that the optical depths of 6.92 keV escaping photons are between $\sim 10^{-3}$ and 10^{-1} . Thus, the attenuation of this X-ray line is expected to be $\lesssim 10\%$ for flares occurring at low heliocentric angles. However, the line attenuation can be much higher for flares near the solar limb.

A serious complication to the X-ray line measurements could arise from the confusion of the radioactivity lines with the intense thermal emission from the flare plasma. In particular, this could prevent a detection of the delayed X-ray lines for hours after the impulsive flaring phase, until the thermal emission has become sufficiently low. The necessary distinction of thermal and nonthermal photons would certainly benefit from an X-ray instrument with high spectral resolution, because $K\alpha$ lines from neutral to low-ionized Fe, Co or Ni are not expected from thermal plasmas at ionization equilibrium. The neutral Co line at 6.92 keV could still be confused, however, with the thermal $K\alpha$ line of Fe XXVI at 6.97 keV. The neutral Fe $K\alpha$ line at 6.40 keV is commonly observed during large solar flares (e.g. Culhane et al. 1981), as a result of photoionization by flare X-rays and collisional ionization by accelerated electrons (e.g. Zarro, Dennis, & Slater 1992). However, this nonthermal line emission is not expected to extend beyond the impulsive phase.

A near future detection of delayed nuclear gamma-ray lines is perhaps more probable. We see in Table 4 that at $t=30$ min after the flare, the brightest gamma-ray line (after the 511 keV line) is at 1434 keV from the β^+ decay of the isomeric state $^{52}\text{Mn}^m$ into ^{52}Cr . The flux of this line is predicted to significantly increase as the accelerated particle spectrum becomes harder, because it is mainly produced from Fe spallation reactions at relatively high energies, >10 MeV nucleon $^{-1}$ (Figure 4). For $t \gtrsim 3$ hours, the radioactivity of $^{52}\text{Mn}^m$ ($T_{1/2}=21.1$ min) has become negligible and the 1434 keV line essentially results from the decay of the ground state $^{52}\text{Mn}^g$ ($T_{1/2}=5.59$ days). Thus, this line remains significant for several days after the flare. However, for $t \gtrsim 2$ days, the most intense line could be at 846.8 keV from ^{56}Co decay, depending on the spectral index s (see Table 6). Additional important gamma-ray lines during the first hour are at 1332 and 1792 keV from the radioactivity of ^{60}Cu . During the first two days, one should also look for the line at 931.1 keV from the radioactivity of ^{55}Co and for those at 1369 and 2754 keV from ^{24}Na decay.

We now discuss the influence of the accelerated ion composition on the delayed line emission. In Figure 12, we show calculated fluences of the 846.8 and 1434 keV lines as a function of the

accelerated α/p abundance ratio. They were obtained from the equation

$$\mathcal{F}_l = \int_0^\infty F_l(t) dt = \frac{\mathcal{F}_{4.4+6.1} Q_r f_d I_l^r}{Q_{4.4+6.1}}, \quad (9)$$

where the yields Q_r and $Q_{4.4+6.1}$ were calculated for various proton abundances relative to α -particles and the other accelerated ions. Thus, the predicted fluence variations with accelerated α/p actually show the relative contributions of reactions induced by fast protons. The fluences decrease for decreasing α/p ratio (i.e. increasing proton abundance), because, for $\alpha/p \gtrsim 0.05$, the radioisotopes are predominantly produced by spallation of accelerated heavy nuclei, whose abundances are significantly enhanced in impulsive flares, whereas the ambient ^{12}C and ^{16}O lines largely result from fast proton interactions. This effect is less pronounced for $s=5$, because for this very soft spectrum, the contribution of α -particle reactions to the prompt line emission is more important. Obviously, the detection of any delayed line from a solar flare should furnish valuable information on the accelerated particle composition and energy spectrum. Determination of the accelerated particle composition from spectroscopy of prompt line emission is difficult.

5. Discussion

We have made a detailed evaluation of the nuclear data relevant to the production of radioactive line emission in the aftermath of large solar flares. We have presented updated cross sections for the synthesis of the major radioisotopes by proton, ^3He and α reactions, and have provided theoretical thick-target yields, which allow flux estimates for all the major delayed lines at any time after a gamma-ray flare.

Together with the 846.8 keV line from ^{56}Co decay, whose importance was already pointed out by Ramaty & Mandzhavidze (2000), our study has revealed other gamma-ray lines that appear to be promising for detection, e.g. at 1434 keV from $^{52}\text{Mn}^{g,m}$, 1332 and 1792 keV from ^{60}Cu , 2127 keV from $^{34}\text{Cl}^m$, 1369 and 2754 keV from ^{24}Na , and 931.1 keV from ^{55}Co . The strongest delayed X-ray line is found to be the Co $K\alpha$ at 6.92 keV, which is produced from both the decay of the isomer $^{58}\text{Co}^m$ by the conversion of a K-shell electron and the decay of ^{57}Ni by orbital electron capture. Distinguishing this atomic line from the thermal X-ray emission can be challenging until the flare plasma has significantly cooled down. However, a few hours after the flare the thermal emission will be gone or significantly reduced and the delayed Co $K\alpha$ line will be more easily detected.

Delayed gamma-ray lines could be detected sooner after the end of the impulsive phase, as the prompt nonthermal gamma-ray emission vanishes more rapidly. The lines will be very narrow, because the radioactive nuclei are stopped by energy losses in the solar atmosphere before they decay. Although generally weaker than the main prompt lines, some delayed lines emitted after large flares can have fluences within the detection capabilities of the *RHESSI* spectrometer or future space instruments. Multiple flares originating from the same active region of the sun can build up the radioactivity, thus increasing the chance for detection.

However, a major complication to the measurements can arise from the fact that the same radioactivity lines can be produced in the instrument and spacecraft materials from fast particle interactions. A line of solar origin could sometimes be disentangled from the instrumental line at the same energy by their different time evolutions. But the bombardment of the satellite by solar energetic particles associated with the gamma-ray flare can make this selection more difficult.

A positive detection of delayed radioactivity lines, hopefully with *RHESSI*, would certainly provide unique information on the flare-accelerated particle composition and energy spectrum. In particular, since the enrichment of the accelerated heavy elements can be the major source of the radioisotopes, their detection should furnish a valuable measurement of this enhancement. Thus, a concomitant detection of the two lines at 846.8 and 1434 keV could allow measurement of not only the abundance of accelerated Fe ions, but also of their energy spectrum (see Figure 12).

A future measurement of the decay curve of the electron-positron annihilation line or of other delayed gamma-ray lines would be very useful for studying solar atmospheric mixing. The lines should be strongly attenuated by Compton scattering when the radioactive nuclei plunge deep in the solar interior. The use of several radioisotopes with different lifetimes should place constraints on the extents and timescales of mixing processes in the outer convection zone. In addition, the imaging capabilities of *RHESSI* could allow measurement of the size and development of the radioactive patch on the solar surface. This would provide unique information on both the transport of flare-accelerated particles and dynamics of solar active regions. It is noteworthy that solar radioactivity can be the only way to study flares that had recently occurred over the east limb.

Radioactive nuclei produced in solar flares can also be detected directly if they escape from the sun into interplanetary space. At present, only two long-lived radioisotopes of solar-flare origin have been identified, ^{14}C ($T_{1/2}=5.7\times 10^3$ years, Jull, Lal, & Donahue 1995) and ^{10}Be ($T_{1/2}=1.51\times 10^6$ years, Nishiizumi & Caffee 2001), from measurements of the solar wind implanted in the outer layers of lunar grains. Based on the measured abundances relative to calculated average production rates in flares, a large part of these radioactive species must be ejected in the solar wind and energetic-particle events rather than being mixed into the bulk of the solar convection zone. Detection of solar radioactivities with shorter lifetimes, either directly in interplanetary space or from their delayed line emission, are expected to provide a new insight into the destiny of the nuclei synthesized in solar flares.

We would like to thank Amel Belhout for her assistance in the EMPIRE-II calculations and Jean-Pierre Thibaud for his constructive comments on the manuscript. B. Kozlovsky would like to thank V. Tatischeff and J. Kiener for their hospitality at Orsay and acknowledges the Israeli Science Foundation for support.

REFERENCES

- Balucinska-Church, M., & McCammon, D. 1992, *ApJ*, 400, 699
- Barrandon, J. N., Debrun, J. L., Kohn, A., & Spear, R. H. 1975, *Nucl. Instrum. Methods Phys. Res.*, 127, 269
- Berger, M.J., Coursey, J.S., Zucker, M.A., & Chang, J. 2005, ESTAR, PSTAR, and ASTAR: Computer Programs for Calculating Stopping-Power and Range Tables for Electrons, Protons, and Helium Ions (version 1.2.3), National Institute of Standards and Technology, Gaithersburg, MD (Available: <http://physics.nist.gov/Star>)
- Chupp, E. L., Forrest, D. J., Higbie, P. R., Suri, A. N., Tsai, C., Dunphy, P. P. 1973, *Nature*, 241, 333
- Culhane, J. L., et al. 1981, *ApJ*, 244, L141
- Ditrói, F., Takács, S., Tárkányi, F., & Mahunka, I. 1994, in *Proceeding of the 13th International Conference on the Application of Accelerators in Research and Industry*, Denton, Texas, USA, 7 - 10 Nov. 1994, 103
- Fessler, A., Alfassi, Z. B., & Qaim, S. M. 1994, *Radiochim. Acta*, 65, 207
- Hazan, J.-P., & Blann, M. 1965, *Phys. Rev.*, 137, 1202
- Herman, M., Obložinský, P., Capote, R., Sin, M., Trkov, A., Ventura, A., & Zerkin, V. 2005, in *Proceeding of the International Conference on Nuclear Data for Science and Technology*, 2004, Santa Fe, USA, AIP Conference Proceedings, Volume 769, 1184. See also URL <http://www.nndc.bnl.gov/empire219/>.
- Hintz, N. M., & Ramsey, N. E. 1952, *Phys. Rev. C*, 88, 19
- Hua, X.-M., Ramaty, R., & Lingenfelter, R. E. 1989, *ApJ*, 341, 516
- Hua, X.-M., Kozlovsky, B., Lingenfelter, R., Ramaty, R., & Stupp, A. 2002, *ApJS*, 140, 563
- Iwata, S. J. 1962, *J. Phys. Soc. Japan*, 17, 1323
- Jull, A. J. T., Lal, D., & Donahue, D. J. 1995, *Earth Planet. Sci. Lett.*, 136, 693
- Kiener, J., Gros, M., Tatischeff, V., & Weidenspointner, G. 2006, *A&A*, 445, 725
- King, C. H., Austin, S. M., Rossner, H. H., & Chien, W. S. 1977, *Phys. Rev. C*, 16, 1712
- Klein, A. T. J, Roesch, F., & Qaim, S. M. 2000, *Radiochim. Acta*, 88, 253
- Koning, A. J., Hilaire, S., & Duijvestijn, M. C. 2005, *Proceeding of the International Conference on Nuclear Data for Science and Technology*, Sep. 26 – Oct. 1, 2004, Santa Fe, USA, AIP Conference Proceedings, Volume 769, 1154.

- Korteling, R. G., & Caretto, A. A. 1970, *Phys. Rev. C*, 1, 193
- Kozlovsky, B., Lingenfelter, R. E., & Ramaty, R. 1987, *ApJ*, 316, 801
- Kozlovsky, B., Murphy, R. J., & Ramaty, R. 2002, *ApJS*, 141, 523
- Kozlovsky, B., Murphy, R. J., & Share, G. H. 2004, *ApJ*, 604, 892
- Kuzhevskij, B. M., Gan, W.-Q., & Miroshnichenko, L. I. 2005, *Chin. J. Astron. Astrophys.*, 5, 295
- Lange, H.-J., et al. 1995, *Appl. Radiat. Isot.*, 46, 93
- Lee, D. M., & Markowitz, S. S. 1974, *Radiochim. Acta*, 19, 159
- Lin, R. P., et al. 2003, *ApJ*, 595, L69
- Lodders, K. 2003, *ApJ*, 591, 1220
- Manzhavidze, N., Ramaty, R., & Kozlovsky, B. 1997, *ApJ*, 489, L99
- Manzhavidze, N., Ramaty, R., & Kozlovsky, B. 1999, *ApJ*, 518, 918
- Matsuo, T., Matuszek, J. M., Dudey, N. D., & Sugihara, T. T. 1965, *Phys. Rev.*, 139, 886
- Meadows, J. W., & Holt, R. B. 1951, *Phys. Rev.*, 83, 47
- Mercer, D. J., et al. 2001, *Phys. Rev. C*, 63, 065805
- Michel, R., Brinkmann, G., & Stück, R. 1983a, in *Proceedings of the International Conference on Nuclear Data for Science and Technology, Antwerp, 1982*, edited by K. H. Bockhoff (Reidal, Dordrecht, 1983), 599
- Michel, R., Brinkmann, G., & Stück, R. 1983b, *Radiochim. Acta*, 32, 173
- Michel, R., et al. 1997, *Nucl. Instrum. Methods Phys. Res. B*, 129, 153
- Moskalenko, I. V., Strong, A. W., Ormes, J. F., & Potgieter, M. S. 2002, *ApJ*, 565, 280
- Muramatsu, H., Shirai, E., Nakahara, H., & Murakami, Y. 1978, *Appl. Radiat. Isot.*, 29, 611
- Murphy, R. J., Ramaty, R., Kozlovsky, B., & Reames, D. V. 1991, *ApJ*, 371, 793
- Murphy, R. J., Share, G. H., Skibo, J. G., & Kozlovsky, B. 2005, *ApJS*, 161, 495
- Nishiizumi, K., & Caffee, M. W. 2001, *Science*, 294, 352
- Parizot, E., & Lehoucq, R. 1999, *A&A*, 346, 211
- Pierce, T. E., & Blann, M. 1968, *Phys. Rev.*, 173, 390

- Ramaty, R., & Mandzhavidze, N. 2000, in IAU Symp. 195, Highly Energetic Physical Processes and Mechanisms for Emission from Astrophysical Plasmas, ed. P. C. H. Martens, S. Tsuruta, & M. A. Weber (San Francisco: ASP), 123
- Ramaty, R., Mandzhavidze, N., & Kozlovsky, B. 1996, in AIP Conf. Proc. 374, High-Energy Solar Physics, ed. R. Ramaty, N. Mandzhavidze, & X.-M. Hua (Woodbury: AIP), 172
- Ramaty, R., Mandzhavidze, N., Kozlovsky, B., & Murphy, R. J. 1995, ApJ, 455, L193
- Read, S., & Viola, V. 1984, At. Data Nucl. Data Tables 31, 359
- Reames, D. V. 1999, Space Sci. Rev., 90, 413
- Reames, D. V., Meyer, J.-P., & von Roseninge, T. T. 1994, ApJS, 90, 649
- Reeder, P. L. 1969, Phys. Rev., 178, 1795
- Reuland, D. J., & Caretto, A. A. 1969, J. Inorg. Nucl. Chem., 31, 1915
- Rizvi, I. A., Bhardwaj, M. K., Ansari, M. A., & Chaubey, A. K. 1989, Can. J. Phys., 67, 1091
- Share, G. H., & Murphy, R. J. 1995, ApJ, 452, 933
- Share, G. H., & Murphy, R. J. 1997, ApJ, 485, 409
- Share, G. H., & Murphy, R. J. 1998, ApJ, 508, 876
- Share, G. H., & Murphy, R. J. 2001, in GAMMA 2001: Gamma-Ray Astrophysics 2001, edited by Steven Ritz, Neil Gehrels, and Chris R. Shrader, AIP Conf. Proc. No. 587 (AIP, Melville, NY), 603
- Share, G. H., Murphy, R. J., & Ryan, J. 1997, in AIP Conf. Proc. 410, Proc. Fourth Compton Symp., ed. C. D. Dermer, M. S. S. Strickman, & J. D. Kurfess (New York: AIP), 17
- Silberberg, R., & Tsao, C. H. 1973, ApJS, 25, 315
- Silberberg, R., Tsao, C. H., & Barghouty, A. F. 1998, ApJ, 501, 911
- Sudár, S., & Qaim, S. M. 1994, Phys. Rev. C, 53, 2885
- Takács, S., Tárkányi, F., Fessler, A., Alfassi, Z. B., & Qaim, S. M. 1995, Appl. Radiat. Isot., 46, 249
- Takács, S., Tárkányi, F., & Kovacs, Z. 1996, Nucl. Instrum. Methods Phys. Res. B, 113, 424
- Takács, S., Vasváry, L., & Tárkányi, F. 1994, Nucl. Instrum. Methods Phys. Res. B, 89, 88
- Tárkányi, F., Ditrói, F., & Takács 2003a, Nucl. Instrum. Methods Phys. Res. B, 211, 312

- Tárkányi, F., Ditrói, F., Takács, S., Szelecsényi, F., Hermanne, A., & Sonck, M. 2003b, Nucl. Instrum. Methods Phys. Res. B, 207, 381
- Tárkányi, F. Szelecsényi, F., & Kopecky, P. 1991, Appl. Radiat. Isot., 42, 513
- Tripathi, R. K., Cucinotta, F. A., Wilson, J. W. 1996, Nucl. Instrum. Methods Phys. Res. B, 117, 347
- Tripathi, R. K., Cucinotta, F. A., Wilson, J. W. 1999, Nucl. Instrum. Methods Phys. Res. B, 155, 349
- Vestrand, W. T., Share, G. H., Murphy, R. J., Forrest, D. J., Rieger, E., Chupp, E. L., & Kanbach, G. 1999, ApJS, 120, 409
- Watanabe, M., Nakahara, H., & Murakami, Y. 1979, Appl. Radiat. Isot., 30, 625
- West, H. I., Lanier, R. G., & Mustafa, M. G. 1987, Phys. Rev. C, 35, 2067
- Wing, J., & Huizenga, J. R. 1962, Phys. Rev., 128, 280
- Zarro, D. M., Dennis, B. R., & Slater, G. L. 1992, ApJ, 391, 865

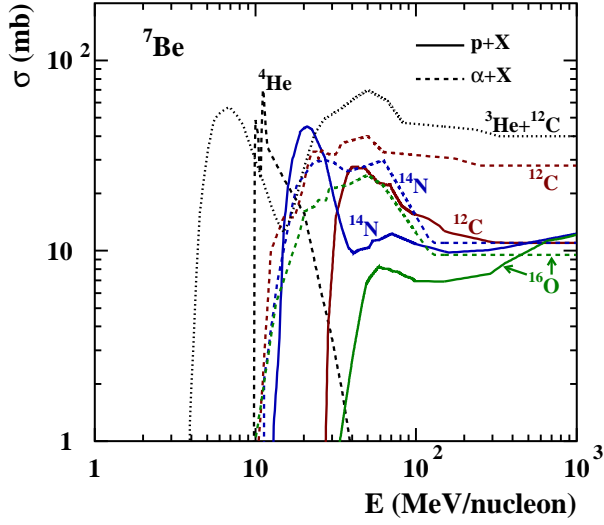


Fig. 1.— Cross sections for the production of ${}^7\text{Be}$ from ${}^3\text{He}$ interactions with ${}^{12}\text{C}$, the ${}^4\text{He}(\alpha, n){}^7\text{Be}$ reaction, and proton and α reactions with ${}^{12}\text{C}$, ${}^{14}\text{N}$ and ${}^{16}\text{O}$. See the electronic edition of the Journal for a color version of this figure.

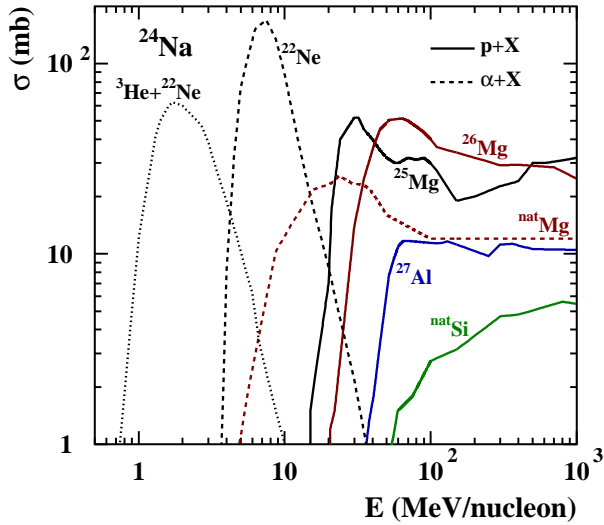


Fig. 2.— Cross sections for the production of ${}^{24}\text{Na}$ from proton reactions with ${}^{25}\text{Mg}$, ${}^{26}\text{Mg}$, ${}^{27}\text{Al}$ and natSi , α reactions with ${}^{22}\text{Ne}$ and natMg , and ${}^3\text{He}$ interactions with ${}^{22}\text{Ne}$. See the electronic edition of the Journal for a color version of this figure.

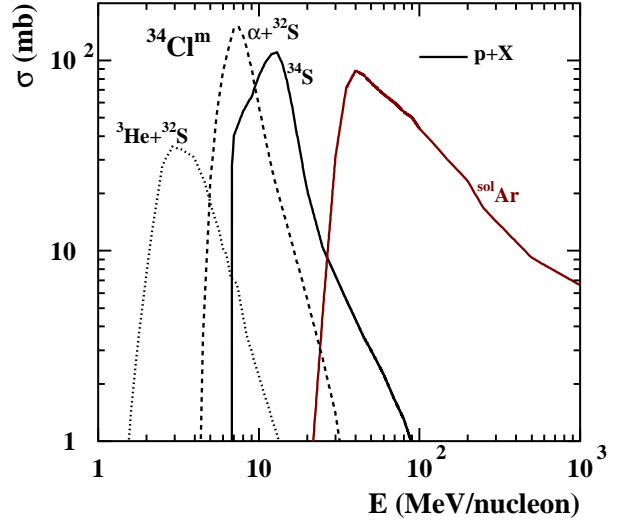


Fig. 3.— Cross sections for the production of ${}^{34}\text{Cl}^m$ from proton reactions with ${}^{34}\text{S}$ and Ar of solar isotopic composition (see text), and ${}^3\text{He}$ and α reactions with ${}^{32}\text{S}$. See the electronic edition of the Journal for a color version of this figure.

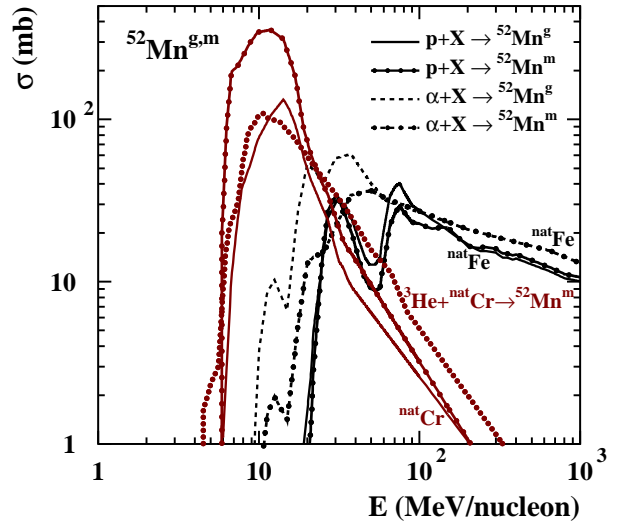


Fig. 4.— Cross sections for the production of ${}^{52}\text{Mn}^g$ and ${}^{52}\text{Mn}^m$ from proton reactions with natCr and natFe , ${}^3\text{He}$ reactions with natCr and α reactions with natFe . See the electronic edition of the Journal for a color version of this figure.

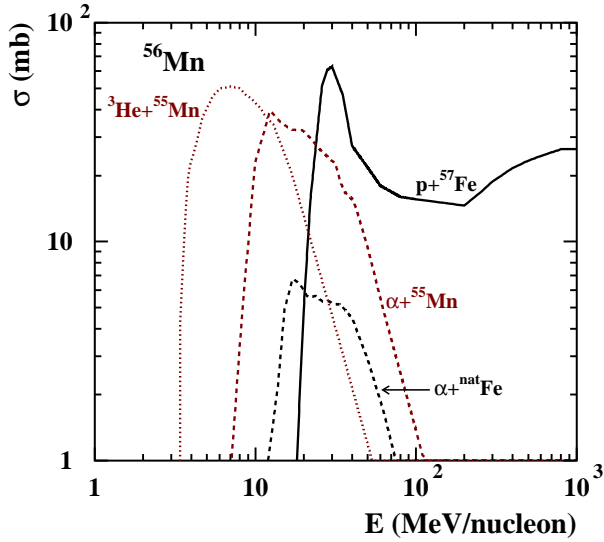


Fig. 5.— Cross sections for the production of ^{56}Mn from ^3He and α reactions with ^{55}Mn , α reactions with $^{\text{nat}}\text{Fe}$, and the $^{57}\text{Fe}(p,2p)^{56}\text{Mn}$ reaction. See the electronic edition of the Journal for a color version of this figure.

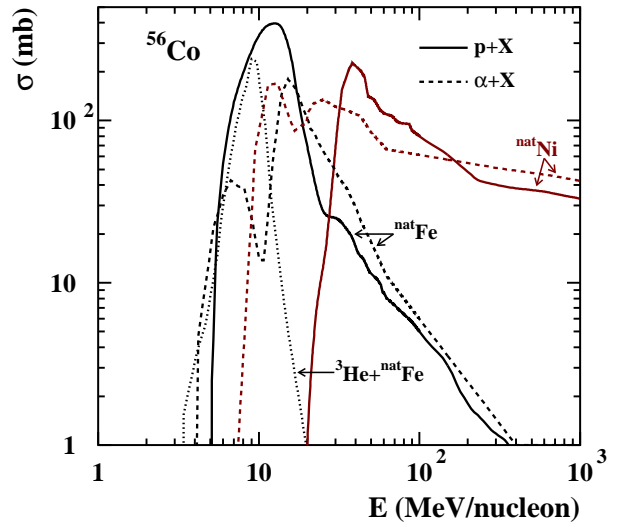


Fig. 7.— Cross sections for the production of ^{56}Co from proton and α reactions with $^{\text{nat}}\text{Fe}$ and $^{\text{nat}}\text{Ni}$, and ^3He reactions with $^{\text{nat}}\text{Fe}$. See the electronic edition of the Journal for a color version of this figure.

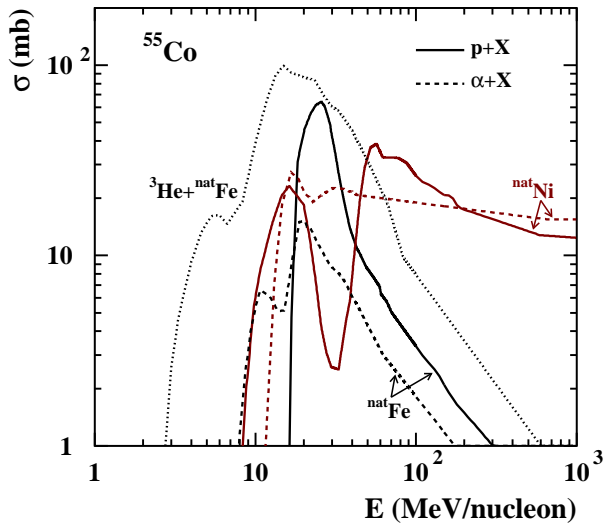


Fig. 6.— Cross sections for the production of ^{55}Co from proton and α reactions with $^{\text{nat}}\text{Fe}$ and $^{\text{nat}}\text{Ni}$, and ^3He reactions with $^{\text{nat}}\text{Fe}$. See the electronic edition of the Journal for a color version of this figure.

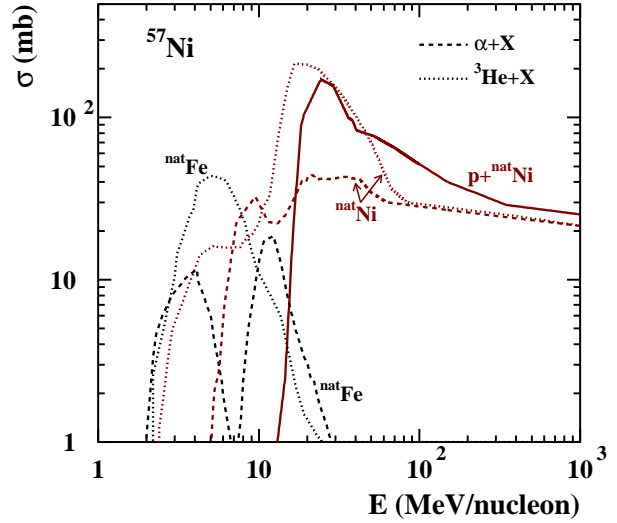


Fig. 8.— Cross sections for the production of ^{57}Ni from ^3He and α reactions with $^{\text{nat}}\text{Fe}$ and $^{\text{nat}}\text{Ni}$, and proton reactions with $^{\text{nat}}\text{Ni}$. See the electronic edition of the Journal for a color version of this figure.

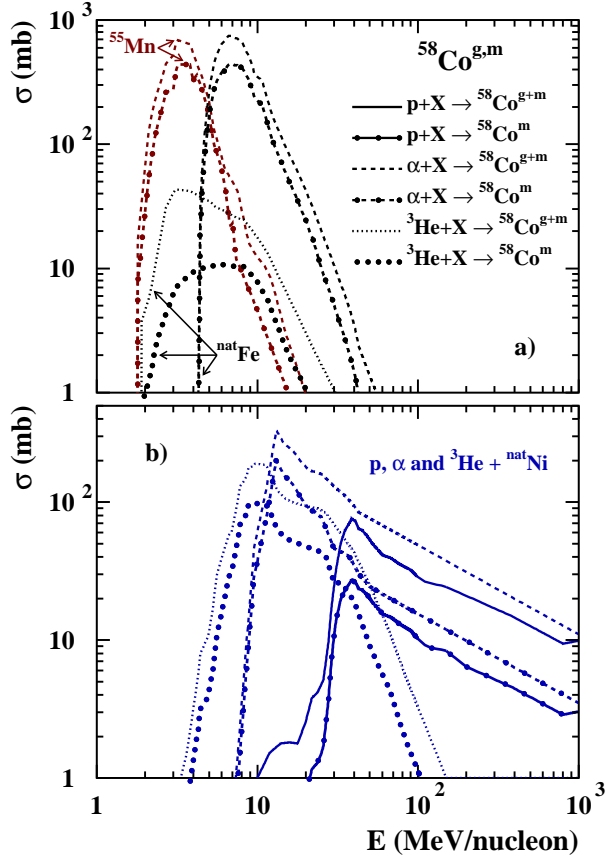


Fig. 9.— Cross sections for the total production of ^{58}Co (i.e. both $^{58}\text{Co}^g$ and $^{58}\text{Co}^m$) and of $^{58}\text{Co}^m$ from (a) α reactions with ^{55}Mn and ^{nat}Fe , as well as ^3He reactions with ^{nat}Fe , and (b) proton, ^3He and α reactions with ^{nat}Ni . See the electronic edition of the Journal for a color version of this figure.

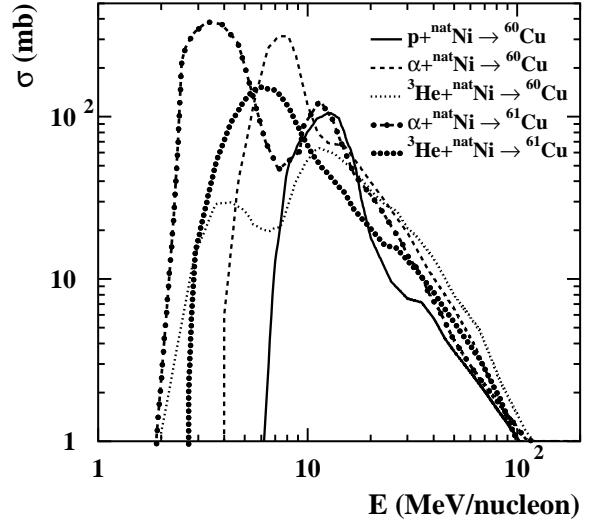


Fig. 10.— Cross sections for the production of ^{60}Cu and ^{61}Cu from proton, ^3He and α reactions with ^{nat}Ni .

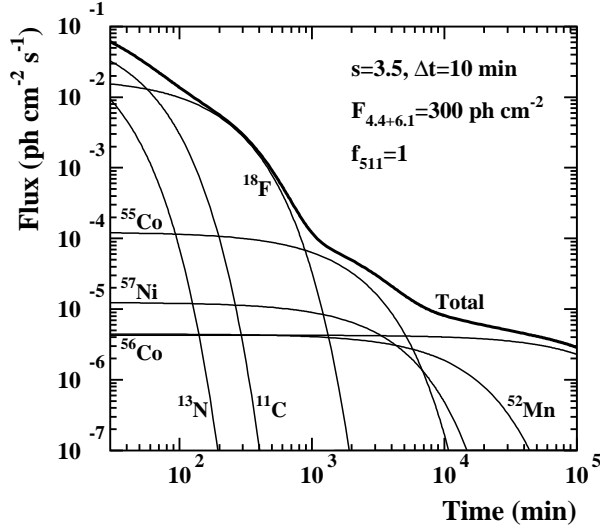


Fig. 11.— Time dependence of the 511 keV line flux with the contributions of the main β^+ -emitters, for a spectral index $s=3.5$ and a flare duration $\Delta t=10$ min. The calculations are normalized to a total fluence of 300 photons cm^{-2} emitted during the gamma-ray flare in the sum of the 4.44 and 6.13 MeV ambient ^{12}C and ^{16}O deexcitation lines. The positron to annihilation-line photon conversion factor $f_{511}=1$. Line attenuation in the solar atmosphere is not taken into account.

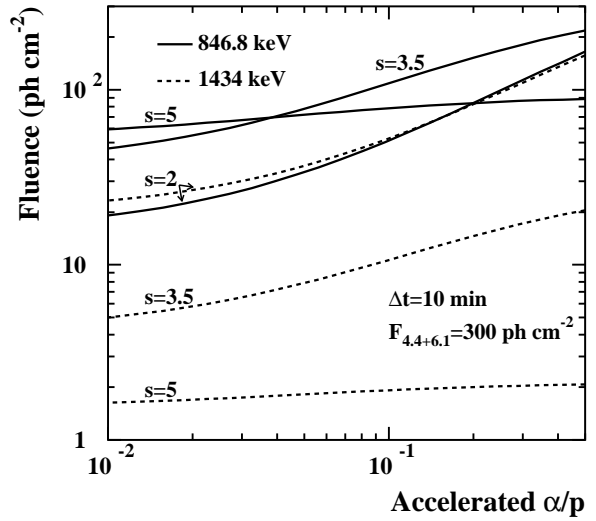


Fig. 12.— Total fluences (eq. [9]) of the delayed lines at 846.8 keV (solid curves) and 1434 keV (dashed curves) as a function of the accelerated α/p abundance ratio (see text), for $s=2, 3.5$ and 5 . The calculations are normalized to a total fluence of 300 photons cm^{-2} emitted during the gamma-ray flare in the sum of the 4.44 and 6.13 MeV ambient ^{12}C and ^{16}O deexcitation lines.

Table 1. Radioactive X- and gamma-ray line emitters ordered by lifetime

Isotope	Half-life ^a	Photon energy (keV) and intensity (%) ^b
¹³ N	9.965 (4) m	511 (99.8)
¹¹ C	20.385 (20) m	511 (99.8)
⁵² Mn ^m	21.1 (2) m	511 (98.2), 1434 (99.8)
⁶⁰ Cu	23.7 (4) m	7.47 (2.5), 511 (93.0), 826.4 (21.7), 1332 (88.0), 1792 (45.4)
³⁴ Cl ^m	32.00 (4) m	146.4 (40.5), 511 (54.3), 1177 (14.1), 2127 (42.8), 3304 (12.3)
⁴⁷ V	32.6 (3) m	511 (96.5)
⁶³ Zn	38.47 (5) m	8.04 (2.5), 511 (92.7)
⁴⁹ Cr	42.3 (1) m	4.95 (2.5), 62.3 (16.4), 90.6 (53.2), 152.9 (30.3), 511 (92.6)
⁵¹ Mn	46.2 (1) m	511 (97.1)
¹⁸ F	109.77 (5) m	511 (96.7)
⁵⁶ Mn	2.5789 (1) h	846.8 (98.9), 1811 (27.2), 2113 (14.3)
⁴⁵ Ti	184.8 (5) m	4.09 (2.3), 511 (84.8)
⁶¹ Cu	3.333 (5) h	7.47 (12.6), 283.0 (12.2), 511 (61.0), 656.0 (10.8)
⁴³ Sc	3.891 (12) h	372.9 (22.5), 511 (88.1)
⁴⁴ Sc	3.97 (4) h	511 (94.3), 1157 (99.9)
⁵² Fe	8.275 (8) h	5.90 (11.2), 168.7 (99.2), 511 (55.5)
⁵⁸ Co ^m	9.04 (11) h	6.92 (23.8)
²⁴ Na	14.9590 (12) h	1369 (100), 2754 (99.9)
⁵⁵ Co	17.53 (3) h	6.40 (6.5), 477.2 (20.2), 511 (76.0), 931.1 (75.0), 1408 (16.9)
⁵⁷ Ni	35.60 (6) h	6.92 (16.7), 127.2 (16.7), 511 (43.6), 1378 (81.7), 1920 (12.3)
⁵² Mn ^g	5.591 (3) d	5.41 (15.5), 511 (29.6), 744.2 (90.0), 935.5 (94.5), 1434 (100)
⁴⁸ V	15.9735 (25) d	4.51 (8.6), 511 (50.3), 983.5 (100), 1312 (97.5)
⁷ Be	53.22 (6) d	477.6 (10.4)
⁵⁸ Co ^g	70.86 (6) d	6.40 (23.0), 511 (14.9), 810.8 (99.4)
⁵⁶ Co	77.233 (27) d	6.40 (21.8), 511 (19.0), 846.8 (99.9), 1038 (14.2), 1238 (66.9), 1771 (15.5), 2598 (17.3)

^aThe half-life uncertainty is indicated by the number in parenthesis, which represents the uncertainty in the least significant digit(s). The units are: m=minute, h=hour and d=day. The decay data are extracted from the NuDat database, URL <http://www.nndc.bnl.gov/nudat2/>

^bNumber of line photons emitted per 100 radioactive decays, except for the 511 keV positron annihilation line for which the given intensity is for the positron production. All K α -X- and gamma-ray lines with intensities greater than 2 and 10%, respectively, were considered.

Table 2. Radioisotope production reactions

Isotope	Reactions
${}^7\text{Be}$	${}^4\text{He}(\alpha, n)$, ${}^{12}\text{C}(p, x)$, ${}^{12}\text{C}({}^3\text{He}, x)$, ${}^{12}\text{C}(\alpha, x)$, ${}^{14}\text{N}(p, x)$, ${}^{14}\text{N}(\alpha, x)$, ${}^{16}\text{O}(p, x)$, ${}^{16}\text{O}(\alpha, x)$
${}^{24}\text{Na}$	${}^{22}\text{Ne}({}^3\text{He}, p)$, ${}^{22}\text{Ne}(\alpha, pn)$, ${}^{25}\text{Mg}(p, 2p)$, ${}^{26}\text{Mg}(p, 2pn)$, ${}^{\text{nat}}\text{Mg}(\alpha, x)$, ${}^{27}\text{Al}(p, 3pn)^{\text{a}}$, ${}^{\text{nat}}\text{Si}(p, x)$
${}^{34}\text{Cl}^m$	${}^{32}\text{S}({}^3\text{He}, p)$, ${}^{32}\text{S}(\alpha, pn)$, ${}^{34}\text{S}(p, n)$, ${}^{\text{sol}}\text{Ar}(p, x)^{\text{b}}$
${}^{52}\text{Mn}^{g,m}$	${}^{\text{nat}}\text{Cr}(p, x)$, ${}^{\text{nat}}\text{Cr}({}^3\text{He}, x)$, ${}^{52}\text{Mn}^m$ ^c , ${}^{\text{nat}}\text{Fe}(p, x)$, ${}^{\text{nat}}\text{Fe}(\alpha, x)$
${}^{56}\text{Mn}$	${}^{55}\text{Mn}({}^3\text{He}, 2p)$, ${}^{55}\text{Mn}(\alpha, 2pn)$, ${}^{57}\text{Fe}(p, 2p)$, ${}^{\text{nat}}\text{Fe}(\alpha, x)$
${}^{55}\text{Co}$	${}^{\text{nat}}\text{Fe}(p, x)$, ${}^{\text{nat}}\text{Fe}({}^3\text{He}, x)$, ${}^{\text{nat}}\text{Fe}(\alpha, x)$, ${}^{\text{nat}}\text{Ni}(p, x)$, ${}^{\text{nat}}\text{Ni}(\alpha, x)$
${}^{56}\text{Co}$	${}^{\text{nat}}\text{Fe}(p, x)$, ${}^{\text{nat}}\text{Fe}({}^3\text{He}, x)$, ${}^{\text{nat}}\text{Fe}(\alpha, x)$, ${}^{\text{nat}}\text{Ni}(p, x)$, ${}^{\text{nat}}\text{Ni}(\alpha, x)$
${}^{57}\text{Ni}$	${}^{\text{nat}}\text{Fe}(p, x)$, ${}^{\text{nat}}\text{Fe}({}^3\text{He}, x)$, ${}^{\text{nat}}\text{Fe}(\alpha, x)$, ${}^{\text{nat}}\text{Ni}(p, x)$, ${}^{\text{nat}}\text{Ni}({}^3\text{He}, x)$, ${}^{\text{nat}}\text{Ni}(\alpha, x)$
${}^{58}\text{Co}^{g,m}$	${}^{55}\text{Mn}(\alpha, n)$, ${}^{\text{nat}}\text{Fe}({}^3\text{He}, x)$, ${}^{\text{nat}}\text{Fe}(\alpha, x)$, ${}^{\text{nat}}\text{Ni}(p, x)$, ${}^{\text{nat}}\text{Ni}({}^3\text{He}, x)$, ${}^{\text{nat}}\text{Ni}(\alpha, x)$
${}^{60}\text{Cu}$	${}^{\text{nat}}\text{Ni}(p, x)$, ${}^{\text{nat}}\text{Ni}({}^3\text{He}, x)$, ${}^{\text{nat}}\text{Ni}(\alpha, x)$
${}^{61}\text{Cu}$	${}^{\text{nat}}\text{Ni}({}^3\text{He}, x)$, ${}^{\text{nat}}\text{Ni}(\alpha, x)$

^aHere and in the following, the notation "xpn" in the reaction output channel denotes $xp+n$, $(x-1)p+d$ or $(x-2)p+{}^3\text{He}$ (if $x \geq 2$).

^bThe notation ^{sol}Ar means Ar of solar isotopic composition (see text).

^cThe contribution of ${}^3\text{He}+{}^{\text{nat}}\text{Cr}$ collisions to ${}^{52}\text{Mn}^g$ production was safely neglected.

Table 3. Radioisotope production yields

Isotope	Production yields ^a			f_d^b	Ref. ^c
	$s=3.5$	$s=2$	$s=5$		
¹³ N	1.43×10^{-6}	1.49×10^{-5}	8.89×10^{-7}	0.72	1
¹¹ C	2.98×10^{-6}	5.80×10^{-5}	5.12×10^{-6}	0.85	1
⁵² Mn ^m	1.88×10^{-7}	7.42×10^{-6}	2.15×10^{-8}	0.85	2
⁶⁰ Cu	4.24×10^{-8}	1.49×10^{-7}	1.70×10^{-8}	0.87	2
³⁴ Cl ^m	4.09×10^{-8}	4.69×10^{-7}	1.96×10^{-8}	0.90	2
⁴⁷ V	2.34×10^{-8}	1.58×10^{-6}	5.95×10^{-10}	0.90	1
⁶³ Zn	1.02×10^{-8}	7.63×10^{-9}	1.58×10^{-8}	0.92	1
⁴⁹ Cr	1.71×10^{-8}	1.84×10^{-6}	2.27×10^{-10}	0.92	1
⁵¹ Mn	4.08×10^{-8}	1.94×10^{-6}	2.39×10^{-9}	0.93	1
¹⁸ F	2.99×10^{-6}	2.66×10^{-5}	4.99×10^{-6}	0.97	1
⁵⁶ Mn	1.01×10^{-8}	2.52×10^{-7}	1.02×10^{-9}	0.98	2
⁴⁵ Ti	1.46×10^{-0}	1.68×10^{-8}	1.69×10^{-12}	0.98	1
⁶¹ Cu	4.55×10^{-8}	4.50×10^{-8}	7.55×10^{-8}	0.98	2
⁴³ Sc	5.67×10^{-9}	1.94×10^{-8}	6.22×10^{-9}	0.99	1
⁴⁴ Sc	4.29×10^{-0}	2.68×10^{-8}	2.18×10^{-11}	0.99	1
⁵² Fe	1.38×10^{-9}	9.31×10^{-8}	3.35×10^{-11}	0.99	1
⁵⁸ Co ^m	6.15×10^{-7}	1.30×10^{-6}	3.92×10^{-7}	0.99	2
²⁴ Na	9.94×10^{-8}	3.59×10^{-6}	3.64×10^{-8}	1	2
⁵⁵ Co	2.34×10^{-7}	3.18×10^{-6}	2.59×10^{-8}	1	2
⁵⁷ Ni	8.41×10^{-8}	8.76×10^{-7}	7.78×10^{-8}	1	2
⁵² Mn ^g	1.67×10^{-7}	7.24×10^{-6}	1.01×10^{-8}	1	2
⁴⁸ V	4.54×10^{-8}	2.89×10^{-6}	2.22×10^{-9}	1	1
⁷ Be	9.07×10^{-6}	6.33×10^{-5}	2.07×10^{-6}	1	2
⁵⁸ Co ^g	1.01×10^{-6}	2.33×10^{-6}	6.54×10^{-7}	1	2
⁵⁶ Co	3.46×10^{-6}	1.40×10^{-5}	1.21×10^{-6}	1	2
4.44 MeV	2.73×10^{-6}	1.38×10^{-5}	2.34×10^{-6}	-	2
6.13 MeV	2.04×10^{-6}	1.20×10^{-5}	1.76×10^{-6}	-	2

^aNondimensional (eq. [3]). The calculations are normalized to unit number of accelerated protons of energies greater than 5 MeV impinging on the solar thick target. The last two lines of the table give the production yields of the 4.44 and 6.13 MeV deexcitation lines from solar ambient ¹²C and ¹⁶O, respectively.

^bFactor which takes into account the decay of the radioactive isotopes during the flare, assuming a flare duration of 10 min and a steady-state radioisotope production (see eq. [7]).

^cSource of the radioisotope production cross sections– (1) Kozlovsky et al. (1987, 2004); (2) this work.

Table 4. Delayed X- and gamma-ray line fluxes at $t=30$ min

Energy (keV)	Parent nucleus ^a	Line flux (photons cm ⁻² s ⁻¹) ^b		
		$s=3.5$	$s=2$	$s=5$
511	¹¹ C, ¹⁸ F, ¹³ N...	6.09×10^{-2}	1.85×10^{-1}	1.02×10^{-1}
1434	⁵² Mn ^m , ⁵² Mn ^g	2.07×10^{-3}	1.51×10^{-2}	2.74×10^{-4}
1332	⁶⁰ Cu	4.12×10^{-4}	2.67×10^{-4}	1.93×10^{-4}
1792	⁶⁰ Cu	2.13×10^{-4}	1.38×10^{-4}	9.95×10^{-5}
6.92	⁵⁸ Co ^m , ⁵⁷ Ni	1.92×10^{-4}	8.25×10^{-5}	1.44×10^{-4}
2127	³⁴ Cl ^m	1.87×10^{-4}	3.95×10^{-4}	1.04×10^{-4}
146.4	³⁴ Cl ^m	1.76×10^{-4}	3.74×10^{-4}	9.86×10^{-5}
931.1	⁵⁵ Co	1.18×10^{-4}	2.98×10^{-4}	1.53×10^{-5}
826.4	⁶⁰ Cu	1.02×10^{-4}	6.59×10^{-5}	4.75×10^{-5}
90.6	⁴⁹ Cr	8.80×10^{-5}	1.75×10^{-3}	1.36×10^{-6}
1369	²⁴ Na	7.84×10^{-5}	5.23×10^{-4}	3.33×10^{-5}
2754	²⁴ Na	7.83×10^{-5}	5.22×10^{-4}	3.33×10^{-5}
846.8	⁵⁶ Mn, ⁵⁶ Co	6.29×10^{-5}	2.02×10^{-4}	1.39×10^{-5}
1177	³⁴ Cl ^m	6.14×10^{-5}	1.30×10^{-4}	3.43×10^{-5}
3304	³⁴ Cl ^m	5.36×10^{-5}	1.14×10^{-4}	3.00×10^{-5}
152.9	⁴⁹ Cr	5.01×10^{-5}	9.98×10^{-4}	7.76×10^{-7}
477.2	⁵⁵ Co	3.19×10^{-5}	8.02×10^{-5}	4.11×10^{-6}
7.47	⁶¹ Cu, ⁶⁰ Cu	3.02×10^{-5}	1.10×10^{-5}	4.11×10^{-5}
62.3	⁴⁹ Cr	2.71×10^{-5}	5.40×10^{-4}	4.20×10^{-7}
1408	⁵⁵ Co	2.67×10^{-5}	6.71×10^{-5}	3.44×10^{-6}
1378	⁵⁷ Ni	2.31×10^{-5}	4.45×10^{-5}	2.49×10^{-5}
283.0	⁶¹ Cu	1.79×10^{-5}	3.26×10^{-6}	3.45×10^{-5}
6.40	⁵⁵ Co, ⁵⁶ Co, ⁵⁸ Co ^g	1.69×10^{-5}	3.02×10^{-5}	4.57×10^{-6}
656.0	⁶¹ Cu	1.58×10^{-5}	2.89×10^{-6}	3.05×10^{-5}
1238	⁵⁶ Co	1.51×10^{-5}	1.13×10^{-5}	6.16×10^{-6}
935.5	⁵² Mn ^g	1.42×10^{-5}	1.14×10^{-4}	1.00×10^{-6}
744.2	⁵² Mn ^g	1.35×10^{-5}	1.08×10^{-4}	9.54×10^{-7}
1811	⁵⁶ Mn	1.11×10^{-5}	5.08×10^{-5}	1.30×10^{-6}

^aFor lines having multiple progenitors, the latter are given in decreasing order of their contribution to the line flux. For the 511 keV positron annihilation line, only the three main β^+ -emitters are indicated.

^bThe calculations are normalized to a total fluence of 300 photons cm⁻² emitted during the gamma-ray flare in the sum of the 4.44 and 6.13 MeV ambient ¹²C and ¹⁶O deexcitation lines. Decay of the ra-

diisotope during the flare is taken into account with the multiplying factor f_d given in Table 2. The 511 keV line fluxes are obtained with a positron to annihilation-line photon conversion factor $f_{511}=1$. The fluxes of the 6.92, 7.47 and 6.40 keV lines should be taken as upper limits, because photoelectric absorption was not taken into account (see text). Only the lines whose flux is $>10^{-5}$ photons $\text{cm}^{-2} \text{s}^{-1}$ for $s=3.5$ are shown.

Table 5. Delayed X- and gamma-ray line fluxes at $t=3$ hours

Energy (keV)	Parent nucleus ^a	Line flux (photons cm ⁻² s ⁻¹) ^a		
		$s=3.5$	$s=2$	$s=5$
511	¹⁸ F, ¹¹ C, ⁵⁵ Co...	6.44×10^{-3}	1.17×10^{-2}	1.21×10^{-2}
6.92	⁵⁸ Co ^m , ⁵⁷ Ni	1.59×10^{-4}	6.92×10^{-5}	1.19×10^{-4}
931.1	⁵⁵ Co	1.07×10^{-4}	2.70×10^{-4}	1.38×10^{-5}
1369	²⁴ Na	6.98×10^{-5}	4.66×10^{-4}	2.97×10^{-5}
2754	²⁴ Na	6.97×10^{-5}	4.65×10^{-4}	2.97×10^{-5}
846.8	⁵⁶ Co, ⁵⁶ Mn	4.31×10^{-5}	1.11×10^{-4}	1.16×10^{-5}
1434	⁵² Mn ^m , ⁵² Mn ^g	2.97×10^{-5}	2.27×10^{-4}	3.03×10^{-6}
477.2	⁵⁵ Co	2.89×10^{-5}	7.26×10^{-5}	3.72×10^{-6}
1408	⁵⁵ Co	2.42×10^{-5}	6.08×10^{-5}	3.11×10^{-6}
1378	⁵⁷ Ni	2.20×10^{-5}	4.24×10^{-5}	2.37×10^{-5}
6.40	⁵⁵ Co, ⁵⁶ Co, ⁵⁸ Co ^g	1.59×10^{-5}	2.78×10^{-5}	4.45×10^{-6}
1238	⁵⁶ Co	1.51×10^{-5}	1.13×10^{-5}	6.15×10^{-6}
935.5	⁵² Mn ^g	1.40×10^{-5}	1.12×10^{-4}	9.89×10^{-7}
744.2	⁵² Mn ^g	1.33×10^{-5}	1.07×10^{-4}	9.42×10^{-7}
7.47	⁶¹ Cu, ⁶⁰ Cu	1.11×10^{-5}	2.10×10^{-6}	2.12×10^{-5}
283	⁶¹ Cu	1.06×10^{-5}	1.94×10^{-6}	2.05×10^{-5}

^aSame as Table 4.

Table 6. Delayed X- and gamma-ray line fluxes at $t=3$ days

Energy (keV)	Parent nucleus ^a	Line flux (photons cm ⁻² s ⁻¹) ^a		
		$s=3.5$	$s=2$	$s=5$
846.8	⁵⁶ Co, ⁵⁶ Mn	2.20×10^{-5}	1.64×10^{-5}	8.95×10^{-6}
511	⁵⁵ Co, ⁵⁶ Co, ⁵² Mn...	1.91×10^{-5}	5.94×10^{-5}	6.95×10^{-6}
1238	⁵⁶ Co	1.47×10^{-5}	1.10×10^{-5}	6.00×10^{-6}
1434	⁵² Mn ^g , ⁵² Mn ^m	1.04×10^{-5}	8.32×10^{-5}	7.33×10^{-7}

^aSame as Table 4.